

## Stellar Evolution: Comparison of Theory with Observation

Comparison of stellar models with the observations tells us about the interior structure of real stars.

Icko Iben, Jr.

How a star forms and how a star of a given initial mass may approach its end are still unanswered questions. On the other hand, our understanding of those nuclear-burning phases in which a star spends most of its active, luminous life is relatively secure. Puzzles still remain, and the theoretical structure is far from complete, but, on the whole, comparison between the observations and theoretical models of evolving stars engenders confidence. It is my primary purpose here to elaborate my reasons for maintaining this confidence and, at the same time, to point out a puzzle which remains and, by remaining, helps make stellar evolution an active and exciting field.

### Evolution of a Typical Metal-Rich Star

At the surface of most of the stars in our galaxy, hydrogen and helium are much more abundant than all of the other elements put together. For example, for every gram of hydrogen and helium near the surface of the sun, there are only a few hundredths of a gram of elements heavier than helium. In the great majority of stars in our galaxy, the surface abundances of the heavier elements are considerably small-

er than they are at the surface of the sun. We therefore call the sun a metal-rich star, despite the fact that metals in the sun are much less abundant than hydrogen and helium. In the total makeup of our galaxy, metal-poor stars considerably outnumber metal-rich stars. However, many of the brightest stars in the disk of our galaxy and in the neighborhood of our sun are metal-rich. In particular, this is true of many of the brightest stars in the familiar constellations such as Orion and Taurus. If for no other reason, this makes metal-rich stars, for me, highly interesting subjects of study.

For definiteness, I shall focus on a star of mass five times that of the sun ( $5 M_{\odot}$ ) (1) and suppose that the abundances of the elements in the initial model are roughly similar to those near the surface of the sun. To be specific, out of every gram of stellar matter, I shall suppose that hydrogen ( $H^1$ ), helium ( $He^4$ ), carbon ( $C^{12}$ ), nitrogen ( $N^{14}$ ), and oxygen ( $O^{16}$ ) contribute a mass of  $0.71$ ,  $0.27$ ,  $3.6 \times 10^{-3}$ ,  $1.2 \times 10^{-3}$ , and  $1.1 \times 10^{-2}$  gram, respectively. I shall lump the remainder of the elements together rather indiscriminately to complete the specification of initial composition.

For the purpose of checking the adequacy of the theoretical models, the most important result of an evolutionary calculation is a time-dependent re-

lationship between observable quantities. The changing relationship between the surface temperature and luminosity of the  $5-M_{\odot}$  model star is most conveniently described by means of a path in the so-called Hertzsprung-Russell diagram, as shown in Fig. 1. In this diagram, the logarithm of the star's energy output, or luminosity  $L$ , is related to the logarithm of the star's surface temperature  $T_e$ . Luminosity is given in units of the sun's luminosity,  $L_{\odot} = 3.86 \times 10^{33}$  ergs per second, and surface temperature is in degrees Kelvin. As time progresses, luminosity and surface temperature of the model star vary along the path in the direction of the arrows. Logarithms in Fig. 1 are to the base 10. Thus, at point 1 in Fig. 1, the  $5-M_{\odot}$  model emits 580 times as much energy per second as the sun does and is characterized by a surface temperature of about  $18,600^{\circ}K$ . At point 2, the  $5-M_{\odot}$  star emits, at a surface temperature of about  $15,700^{\circ}K$ , 1000 times as much energy per second as the sun does.

The surface temperature of a star is related to its color. The sun, whose surface temperature is roughly  $6000^{\circ}K$  ( $\log T_e = 3.78$ ), appears yellow. A star with a surface temperature of  $4500^{\circ}K$  ( $\log T_e = 3.65$ ) would appear red, and a star with a surface temperature greater than  $10,000^{\circ}K$  ( $\log T_e = 4.0$ ) would appear blue or whitish-blue. Thus, the higher the surface temperature, the bluer the star; the lower the surface temperature, the redder the star. For ease in speaking, it is often convenient to replace a statement concerning surface temperature and luminosity by one involving color and brightness. For example, one may say that, between points 5 and 6 in Fig. 1, the  $5-M_{\odot}$  model star evolves toward the red and becomes dimmer. Between points 6 and 7, the model star brightens and becomes redder still.

Numbered circles along the path in Fig. 1 denote boundaries of easily distinguished phases. A description of several phases and points is supplied in Fig. 1, and the time spent by the star in these phases is also indicated.

The author is associate professor of physics at Massachusetts Institute of Technology, Cambridge.

## Hydrogen Burning in the Core

The  $5-M_{\odot}$  star spends the major portion of its active life between points 1 and 2, burning hydrogen in a convective core. During this phase the fraction of the star's mass contained in the convective core decreases steadily from an initial 22 percent to about 8 percent. Within the core, energy is carried primarily by convection and matter is thoroughly mixed. Energy is transported from the core edge to the surface primarily by radiation.

Within the convective core, hydrogen is converted into helium by means of two distinct sets of reactions, the so-called  $p-p$  reactions and the CN-cycle reactions (2). In the  $5-M_{\odot}$  star, the CN-cycle reactions are by far the more important energy producers. The cycle consists of successive proton capture reactions and beta decays which transform  $C^{12}$  into  $N^{14}$  and  $N^{14}$  back into  $C^{12}$  plus a  $He^4$  nucleus. As a result of similar reactions,  $O^{16}$  and two protons are converted to  $N^{14}$  and  $He^4$ .

At the beginning of the hydrogen-burning phase, the rate at which  $C^{12}$  is destroyed in the interior by proton capture is higher than the rate at which it is created as a consequence of proton reactions with  $N^{14}$ . On the other hand, the rate at which  $N^{14}$  is created at first exceeds the rate at which it is destroyed. The net result is that the

abundance of  $N^{14}$  increases at the expense of  $C^{12}$  until all of the reactions are in equilibrium. In equilibrium,  $N^{14}$  is approximately 100 times more abundant than  $C^{12}$ . Very early in the phase of core hydrogen burning,  $C^{12}$  and  $N^{14}$  reach equilibrium values throughout the inner 40 percent of the star's mass. This means that, in the inner two-fifths of the star, almost all of the original  $C^{12}$  has been converted into  $N^{14}$ . This result should not be interpreted to mean that, once equilibrium has been achieved, nuclear energy is produced in significant amounts within the entire inner two-fifths of the star. Rapid energy production occurs only within the inner 5 to 10 percent of the star's mass.

During most of the phase of hydrogen burning in the core, matter near the stellar center contracts. This is a consequence of the decrease in the number of particles per gram in the convective core, brought about by the conversion of hydrogen into helium. A portion of the gravitational energy liberated during contraction is converted into increased thermal motions, so that matter in the energy-producing region of the star heats as it contracts. Because of rising temperatures and densities, the rate of energy production continues to increase and the star's luminosity rises even as the nuclear fuel is being depleted.

During the passage between points 1 and 2 of Fig. 1, the stellar envelope expands to accommodate the increased flow of energy from the interior. As a result of expansion, matter in the envelope also cools. The radius (3) of the star gradually increases from about 2.4 times the sun's radius to 4.25 times the sun's radius.

As the hydrogen abundance near the center becomes smaller and smaller, the stellar core contracts and heats more rapidly. Eventually, just beyond point 2 in Fig. 1, all portions of the star begin to contract in order to keep step with the rapidly contracting core. Between points 2 and 3 the star suffers an overall contraction. Concurrently, the convective core diminishes rapidly in size, finally disappearing between points 3 and 4 at the same time that the central abundance of hydrogen becomes effectively zero.

Between points 3 and 4, the region of major production of nuclear energy shifts from near the center, where hydrogen becomes exhausted, to regions away from the center, where hydrogen is abundant. The details of this shift are rather complex. Suffice it to say that, by the time the star reaches point 4, hydrogen is exhausted over the inner 7 percent of the star's mass. Matter in the hydrogen-exhausted core becomes nearly isothermal.

Between points 4 and 5, production of nuclear energy occurs in a fairly thick shell containing approximately 5 percent of the star's mass. The shell moves slowly outward through the star, adding more mass to the hydrogen-exhausted core.

## To the Giant Branch

As the star approaches point 5, the mass of the hydrogen-exhausted core becomes approximately 10 percent of the star's mass. Thereafter, the pressure balance within the isothermal core cannot be maintained simply by an increase in density from the inner edge of the shell to the center. As a result, the core begins to contract rapidly and to heat up preferentially toward the center. Although matter in the energy-producing shell is now drawn more rapidly than before to higher temperatures and densities, the mass of the shell within which significant nuclear-energy production occurs begins to decrease. Between points 5 and 6, the rate at which temperatures and densi-

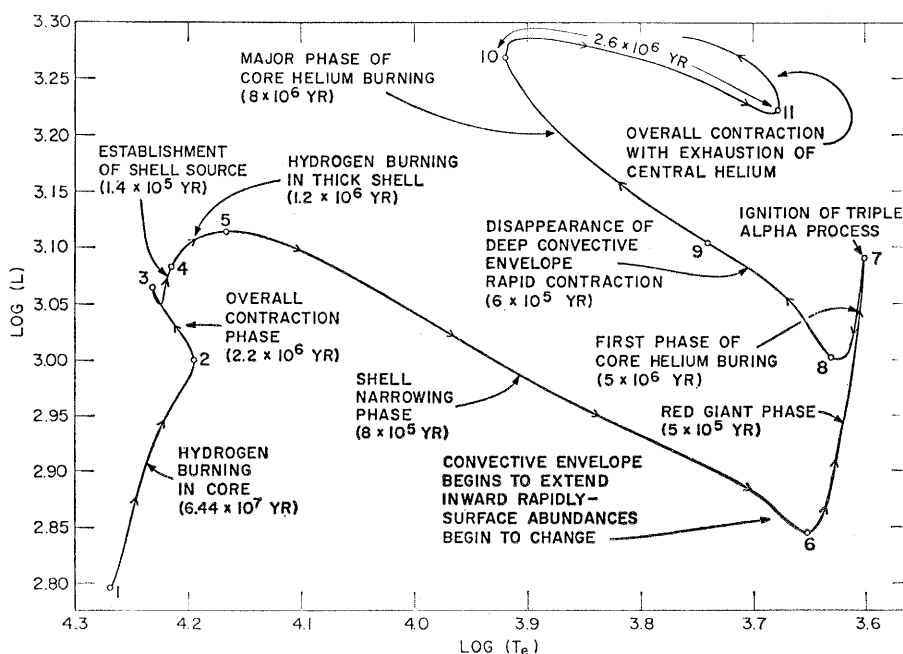


Fig. 1. The evolutionary path of a  $5-M_{\odot}$  star in the Hertzsprung-Russell diagram. Luminosity  $L$  is in units of the sun's luminosity  $L_{\odot}$  ( $= 3.86 \times 10^{38}$  ergs per second) and surface temperature  $T_e$  is in degrees Kelvin. Traversal times between labeled points are given in years.

ties increase within the shell is not sufficient to offset the rate at which the shell narrows, and the total rate of nuclear-energy production decreases with time. The decline in the rate of nuclear-energy production is, however, not solely responsible for the drop in luminosity. Matter in the stellar envelope is expanding, and the stellar radius is increasing rapidly. Some of the energy which is required to expand the matter in the region between the shell and the surface is supplied by the shell. The net amount of energy reaching the surface from the shell is consequently reduced.

Within the expanding and cooling envelope, radiation filters with increasing difficulty from the shell to the surface. Shortly before the star reaches point 6, convection begins to be the dominant mode of energy transport in a growing region extending inward from just below the surface.

On the other hand, between the outer edge of the growing convective envelope and the surface (in the so-called photosphere) matter becomes less and less opaque to radiation as surface temperature drops. Hence, as the surface temperature of the star decreases, beyond point 6, the luminosity of the star begins to increase. The increase in luminosity is accomplished in two ways. Within the convective portion of the envelope, the energy required for expansion is supplied entirely by thermal energy already in the envelope. Thus, as the mass of the convective envelope increases, the nuclear source delivers a larger fraction of its output to the surface. At the same time, the rate of nuclear-energy production in the shell increases.

The path between points 6 and 7 is called the red-giant branch—red because a star in this region of the Hertzsprung-Russell diagram appears red, and giant because the radius of a star here is considerably larger than the radius it has near the main sequence. Along the red-giant branch, stellar radius increases roughly as the square root of the luminosity. At the tip of the red-giant branch (point 7), the radius of the  $5-M_{\odot}$  star is about 74 times the radius of the sun.

As the star's luminosity *increases* along the red-giant branch, the mass within which nuclear energy is produced continues to *decrease*. We can put this another way: the smaller the mass of the energy-producing region, the larger its energy output! The solu-

tion to this apparent paradox rests in the fact that an increase in temperatures and densities within the shell more than offsets the decrease in shell size.

As the star evolves between points 6 and 7, convection covers more and more of the outer mass of the star, reaching almost to the hydrogen-burning shell at point 7. As convection extends into the region where most of the original  $C^{12}$  has been converted into  $N^{14}$ , mixing begins to carry  $N^{14}$  outward and  $C^{12}$  inward. As the convective envelope grows, the abundance of  $N^{14}$  in the envelope gradually increases, while the abundance of  $C^{12}$  drops. The ratio of  $N^{14}$  to  $C^{12}$  in the surface of the star, where it *might* be observed by the spectroscopist, therefore increases between points 6 and 7. Beyond point 7, the mass in the convective envelope begins to decrease and the surface ratio of  $N^{14}$  to  $C^{12}$  ceases to change.

### Helium Burning in the Core

When the star reaches point 7, central temperatures and densities have become sufficiently high that nuclear burning near the center, by way of the so-called triple-alpha process, begins to alter the course of evolution (4). The net result of the triple-alpha process is the fusion of three helium nuclei to form a carbon nucleus.

The ignition of the triple-alpha process is mildly explosive. Temperatures and densities near the center at first rise to such values that the rate of nuclear-energy production there exceeds the rate at which energy may be carried out. The energy trapped near the center then forces the central regions to expand. The expansion initiated near the stellar center inhibits the rate at which temperatures and densities rise in the hydrogen-burning shell, which still provides most of the star's energy output. Hence, immediately after the triple-alpha ignition at point 7, the luminosity of the star drops.

Between points 7 and 10, the stellar envelope contracts and surface temperature increases. This behavior may be ascribed to the fact that the major source of nuclear-energy production is still the hydrogen-burning shell. In order for a balance between energy production and energy outflow to be maintained, matter in the shell must be kept at sufficiently high densities and tem-

peratures. Since the stellar core continues to expand as a consequence of the properties of the triple-alpha reactions, maintenance of high densities and temperatures is accomplished only by means of envelope contraction. The contracting envelope heats and compresses the hydrogen-rich matter at the leading edge of the shell.

Envelope contraction is particularly rapid between points 8 and 9. This phase of contraction is not at all closely connected with nuclear-burning processes in the interior. It is associated with the disappearance of envelope convection as a result of the increased efficiency of radiative flow in the heating and condensing envelope. As the dominant mode of energy flow switches from convective to radiative flow, a rapid readjustment of the matter in the envelope is required.

The energy flux produced by helium burning leads to the formation of a convective central region. As  $C^{12}$  increases in the helium-burning core, it combines with helium to form  $O^{16}$ . As temperatures in the convective core continue to rise, the rate of energy production in the core becomes more comparable with the rate of energy production in the shell. Eventually, changes within the core begin to dominate the direction of evolution. Beginning at point 10, the star evolves again through a phase of decreasing surface temperature. Finally, as the abundance of helium in the core becomes smaller and smaller, there ensues a new phase of overall contraction (beginning at point 11), exactly analogous to the phase of overall contraction (points 2 to 3) which precedes the exhaustion of central hydrogen. A study of subsequent evolution is still in progress (5).

### Dependence of Evolutionary Characteristics on Stellar Mass

In Fig. 2, evolutionary tracks in the Hertzsprung-Russell diagram for several metal-rich stars of different mass are shown. The initial composition of all stars represented in Fig. 2 is the same as that for the  $5-M_{\odot}$  star, described in the preceding sections. The solid portions of each track are direct results of my computations (6). The dashed portions are estimates. The time spent by each star in traversing the intervals between successive labeled points is given in Table 1.

## The Main-Sequence Phase

In each case, the intervals between points 1 and 2 correspond to the major phase of hydrogen burning in the core. Since most of each star's nuclear-burning lifetime is spent in the interval 1-2 and since each interval lies within a fairly narrow band in the Hertzsprung-Russell diagram, the phase of core hydrogen burning is also called the main-sequence phase.

The most obvious mass-dependent features of the main-sequence phase are color, luminosity, and lifetime. The more massive the main-sequence star, the bluer it is. The more massive the star, the more luminous it is and the more rapidly it evolves. Over the mass range shown in Fig. 2, the mean stellar luminosity during the main-sequence phase varies with mass according to the rule  $\bar{L} \sim (M/M_{\odot})^n$ , where the index  $n$  varies from about 5, near one solar mass, to about 3, beyond nine solar masses. The main-sequence lifetime varies, very

roughly, as  $t_{MS} \sim 10^{10} \text{ yr } (M/M_{\odot})/(\bar{L}/L_{\odot})$ . The manner in which lifetime depends on mass and luminosity is quite reasonable: the amount of nuclear fuel available is directly proportional to the mass of the star, whereas the rate at which the fuel is exhausted is directly proportional to the luminosity.

Even though structural and evolutionary characteristics of main-sequence stars vary gradually with stellar mass, it is useful to think of any one star as belonging to one of two major families, the so-called upper main sequence and the lower main sequence. The  $5-M_{\odot}$  star already discussed is typical of the upper main sequence, a class which extends (for the composition chosen) from about  $1.9 M_{\odot}$  upward. The most important distinguishing characteristic of upper-main-sequence stars is the occurrence of a relatively large convective core. For stellar masses greater than about  $1.9 M_{\odot}$ , nuclear-energy production is primarily by the CN-cycle reactions and

is highly concentrated toward the center of the convective core. It is the concentration of energy sources toward the center which gives rise to the convective core. Just as in the  $5-M_{\odot}$  case, energy is carried between the outer edge of the core and the stellar surface by radiative diffusion.

From an evolutionary standpoint, the most important consequence of the large convective core in upper-main-sequence stars is that, although the conversion of hydrogen into helium actually occurs only near the center of the convective core, convective mixing insures that the concentrations of hydrogen and helium are independent of position within the core. Thus, as evolution progresses, hydrogen decreases steadily over a region which is large compared to the region of nuclear-energy production, and, toward the end of the phase of hydrogen burning in the core, all upper-main-sequence stars suffer an overall contraction which is reflected in evolutionary tracks by a rapid brightening and increase in surface temperature (points 2 to 3 in Fig. 2).

The sun and the  $1-M_{\odot}$  star in Fig. 2 are typical of lower-main-sequence stars. For the composition chosen, the class of lower-main-sequence stars extends from about  $1.1 M_{\odot}$  to  $0.4 M_{\odot}$ . In these stars, energy production is primarily by the  $p-p$  chains, sequences of reactions which convert hydrogen into helium even in the absence of the elements  $C^{12}$ ,  $N^{14}$ , and  $O^{16}$ .

Just as the presence of a convective core is the primary distinguishing feature of upper-main-sequence stars, so the absence of a convective core is the primary distinguishing feature of lower-main-sequence stars. Energy production by the  $p-p$  chains is spread over a large fraction of the interior, and energy flow does not become so excessive near the center that it cannot be maintained by radiative diffusion.

In contrast to the case for the upper-main-sequence star, the distribution of hydrogen varies *gradually* and steadily through a major portion of the lower-main-sequence star's mass. It is this difference in the distribution of hydrogen through the star at successive intervals that accounts for the difference in the direction of evolutionary tracks during the main-sequence phase. The surface temperature of the upper-main-sequence star decreases steadily as luminosity increases, whereas the sur-

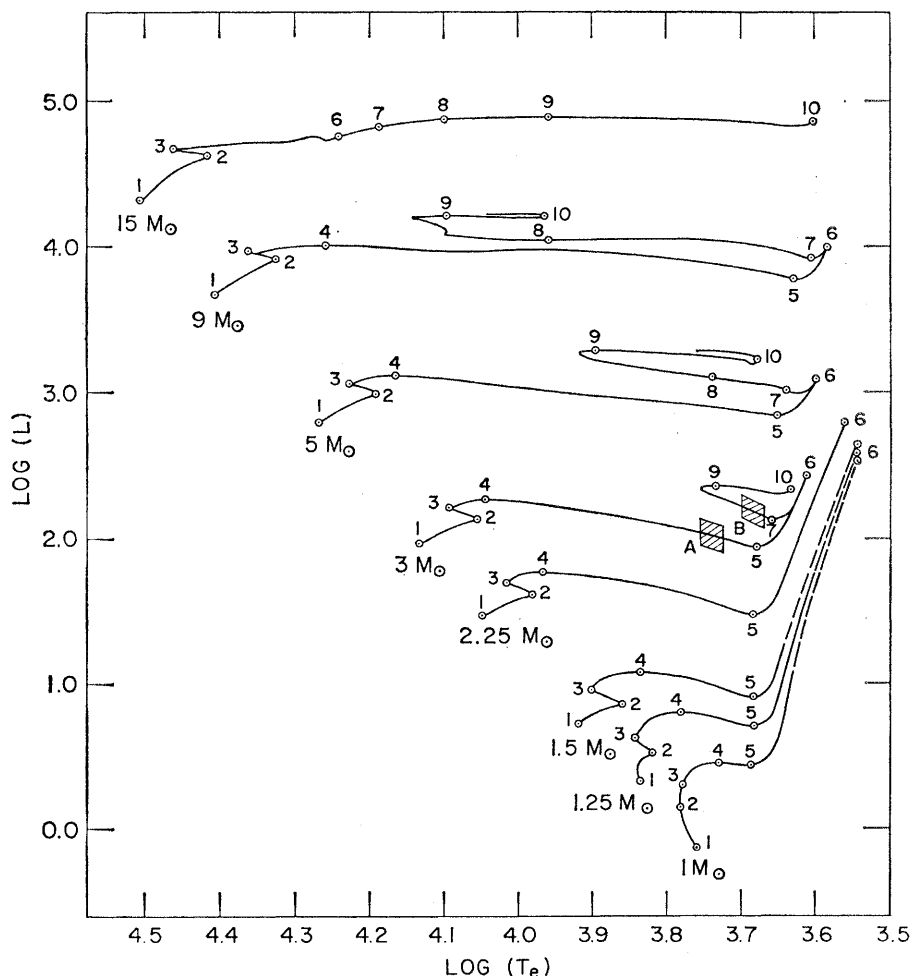


Fig. 2. Paths in the Hertzsprung-Russell diagram for metal-rich stars of mass ( $M/M_{\odot}$ ) = 15, 9, 5, 3, 2.25, 1.5, 1.25, and 1.  $L$  and  $T_e$  as in Fig. 1. Traversal times (in years) between labeled points are given in Table 1.

Table 1. Time (in years) spent by stars of various masses in traversing the intervals between successive labeled points of Fig. 2. The number in parentheses beside each entry indicates the power of 10 to which the entry is to be raised.

Mass ( $M_{\odot}$ )	Interval ( $i-j$ )								
	(1-2)	(2-3)	(3-4)	(4-5)	(5-6)	(6-7)	(7-8)	(8-9)	(9-10)
15	1.010(7)	2.270(5)		7.55 (4)		7.17(5)	6.20(5)	1.9 (5)	3.5 (4)
9	2.114(7)	6.053(5)	9.113(4)	1.477(5)	6.552(4)	4.90(5)	9.50(4)	3.28(6)	1.55(5)
5	6.547(7)	2.173(6)	1.372(6)	7.532(5)	4.857(5)	6.05(6)	1.14(6)	8.90(6)	9.30(5)
3	2.212(8)	1.042(7)	1.033(7)	4.505(6)	4.238(6)	2.51(7)	4.08(7)		6.00(6)
2.25	4.802(8)	1.647(7)	3.696(7)	1.310(7)	3.829(7)				
1.5	1.553(9)	8.10 (7)	3.490(8)	1.049(8)	$\approx 2$ (8)				
1.25	2.803(9)	1.824(8)	1.045(9)	1.463(8)	$\approx 4$ (8)				
1.0	7(9)	2(9)	1.20 (9)	1.57 (8)	$\approx 6$ (8)				

face temperature of the lower-main-sequence star rises over a major portion of the main-sequence phase.

The smoothness of the hydrogen distribution within the lower-main-sequence star is also responsible for the absence of a phase comparable to the phase of overall contraction experienced by upper-main-sequence stars when hydrogen begins to disappear over a large fraction of the energy-producing region. In the lower-main-sequence star, hydrogen vanishes progressively over only small fractions of the nuclear-energy-producing region. Hence the need for rapid contraction and heating to maintain energy production at a sufficiently high level is not as urgent as for the upper-main-sequence star and produces much less drastic effects on observable features.

The region along the main-sequence band corresponding to stars of mass between 1.1 and 1.9  $M_{\odot}$  is one of transition between the two major families. Energy generation both by the  $p-p$  processes and by the CN-cycle processes is important and is not entirely confined to the convective core. As a consequence, evolutionary tracks may exhibit characteristics of both major families. For example, a 1.25- $M_{\odot}$  model star becomes bluer during the early portion of the main-sequence phase, just as the 1- $M_{\odot}$  model star does. However, it eventually evolves toward the red and exhibits a strong phase of overall contraction, as does the typical upper-main-sequence star.

### Post-Main-Sequence Phases

Following the period of hydrogen burning in a thick shell, all metal-rich stars less massive than about 12  $M_{\odot}$  evolve rapidly to the red-giant phase. At the base of the red-giant branch of all such stars (points 5 in Fig. 2), convective motions begin to occur over

a growing portion of the stellar envelope. Convection extends deeper and deeper as the star advances along its giant branch (between points 5 and 6 in Fig. 2). At the tip of the giant branch, convection covers most of the star between the hydrogen-burning shell and the photosphere. In each case, upward motion along the giant branch is ended when helium burning becomes significant in the hydrogen-exhausted core of the star.

The post-main-sequence phase of stars more massive than 12  $M_{\odot}$  is distinguished from that of less massive stars by the fact that temperatures in the stellar core reach sufficiently high values to ignite helium in the core before the star reaches the red-giant phase. For example, during the phase of core helium burning, the 15- $M_{\odot}$  star remains near the main sequence (between points 6 and 9 in Fig. 2) until helium is nearly exhausted in its central regions. It then proceeds to the red-giant phase and will brighten until another nuclear-energy source (carbon- or oxygen-burning) is ignited at the center.

During the giant phase the interior structure of stars less massive than 12  $M_{\odot}$  falls into one of two categories. The bifurcation point in stellar mass occurs at, roughly, 2.25  $M_{\odot}$ . Stars more massive than 2.25  $M_{\odot}$  behave, during the giant stage, qualitatively very much like the 5- $M_{\odot}$  star. In all such stars, pressure in the hydrogen-exhausted core is due predominantly to the thermal motions of electrons and helium nuclei. As the star ascends further up its giant branch, core temperatures and densities rise until helium burning commences in a reasonably quiet manner near the stellar center. All evolutionary tracks during the ensuing phase of core helium burning are topologically equivalent. Quantitative differences are potentially of observational importance. With increasing stellar mass, the following trends are ap-

parent: the phase of rapid envelope contraction (points 7 to 8 in Fig. 2) separating the two major phases of core helium burning becomes more pronounced; the lifetime of the phase of core helium burning relative to the main-sequence lifetime decreases; the maximum surface temperature attained by the star during the phase of core helium burning increases.

During the giant phase in stars less massive than 2.25  $M_{\odot}$ , electrons in the hydrogen-exhausted core are highly degenerate (7) and supply most of the core pressure. This means that the rate of core contraction and heating is inhibited. The growing mass of the hydrogen-exhausted core is supported primarily by a slow increase in core densities. The star climbs quite far upward in the Hertzsprung-Russell diagram before core temperatures become high enough for helium burning to commence at the center. When helium burning does commence, the mass in the hydrogen-exhausted core is approximately 0.4  $M_{\odot}$ , nearly independent of the total mass of the star.

The occurrence of strong electron degeneracy in the core of low-mass stars leads to the phenomenon of helium flashing. The heat generated by the helium-burning reactions *remains* in the degenerate core, causing temperatures to rise. Rising temperatures cause the helium-burning reactions to proceed at an increased rate. The rate of core heating consequently accelerates until eventually the pressure due to the thermal motions of core particles exceeds the pressure due to electron degeneracy. The core then expands and cools as the degeneracy is "lifted." Helium burning then continues quietly in a nondegenerate core in much the same way that it does in more massive stars. However, the evolutionary track during core helium burning is compressed very close to the giant branch, following the trend exhibited by tracks of more massive stars.

## Comparison with the Sun

The comparison between the properties of theoretical model stars and the observable properties of real stars may take several forms.

Conceptually, the simplest comparison one can make is between single stars and individual theoretical models. The most obvious comparison is with the sun, the star for which the maximum amount of information is available. Not only do we know the sun's luminosity, surface temperature, and mass to a relatively high degree of accuracy but we are able to estimate its age as well. By examining the relative abundance of lead isotopes in terrestrial rocks and meteorites we can estimate the age of the earth to be approximately  $4.5 \times 10^9$  years. Assuming the earth, meteorites, and the sun to be approximately coeval, we then know the age of the sun also to be approximately  $4.5 \times 10^9$  years.

The next task is to attempt an estimate of the relative abundances of elements in the sun when it first reached the main sequence. Our only direct knowledge of solar abundances is confined to the matter near the solar surface. As a first approximation, we equate present surface abundances with the abundances in the solar interior prior to the onset of hydrogen burning.

Unfortunately, the relative abundances of the elements in the solar surface are not particularly well known. Spectroscopic data are capable of saying something about the abundances of

metals and of some heavy elements, and of showing that hydrogen is quite abundant relative to all other measurable constituents. Because spectral lines due to helium are not excited at the low temperatures (around  $6000^\circ\text{K}$ ) at the sun's surface, the relative abundance of helium is not determinable spectroscopically. It is necessary to use rocket and satellite measurements of the constituents of the solar wind in order to estimate the relative abundances of helium, hydrogen, and several of the more abundant heavy elements such as  $\text{C}^{12}$ ,  $\text{N}^{14}$ , and  $\text{O}^{16}$ .

Because of uncertainty concerning the initial composition of the sun, the procedure one must adopt is this. Choose an initial abundance distribution consistent with the observations. Evolve the model for 4.5 billion years. Compare the luminosity and surface temperature of the model star with the sun's luminosity and surface temperature. If coincidence does not occur, vary the composition until coincidence is achieved (8). A fairly wide range of initial-composition choices, consistent with the spectroscopic and solar-wind data, leads to the correct model luminosity and surface temperature after 4.5 billion years. There is thus considerable uncertainty concerning the *exact* interior structure of the present sun.

The *approximate* interior characteristics of the sun are illustrated in Fig. 3, where each structure and composition variable shown is scaled in such a way that unity along the vertical axis corresponds to the maximum

value of that variable in the sun. The central density in this model of the sun is about 160 grams per cubic centimeter, and the central temperature is approximately 16 million degrees Kelvin. The initial-composition variables are the same as those chosen for the metal-rich stars described in the preceding two sections. Note that, over the past 4.5 billion years, approximately half of the hydrogen originally present at the sun's center has been converted into helium. This means that, in another 5 billion years or so, the sun will have exhausted its central hydrogen and will be well on the way toward becoming a red giant. As the sun evolves along the red-giant branch, its radius will successively reach the present orbits of Mercury, Venus, and so on. Each planet will be vaporized as it is engulfed, and its material will become a part of the sun.

## Comparison with Capella

As another example, consider the three stars which make up what we call Capella. In the Capella complex, two components, which I shall call Capella A and Capella B, are each of about the same mass, the B component being slightly more massive than  $3 M_\odot$ , the A component being slightly less massive than  $3 M_\odot$ . Components A and B are both luminous red stars, Capella B being slightly redder (having lower surface temperature) and somewhat more luminous than Capella A. In addition, the surface-lithium content of Capella B is considerably less than that of Capella A. All of these facts permit one to identify Capella A as a star which is approaching the base of its red-giant branch, whereas Capella B has already embarked on the extended phase of helium burning in the core coupled with hydrogen burning in a shell.

The approximate location of Capella A and B in the Hertzsprung-Russell diagram are noted in Fig. 2. During the main-sequence phase, lithium is destroyed, by reacting with protons, over the inner 99 percent of both Capella A and B, leaving unburned lithium in only a very thin layer near the surface of each star. Once either star reaches the base of its giant branch, convection begins to extend inward beyond the layer of unburned lithium. Since a fixed quantity of lithium is mixed over a larger and

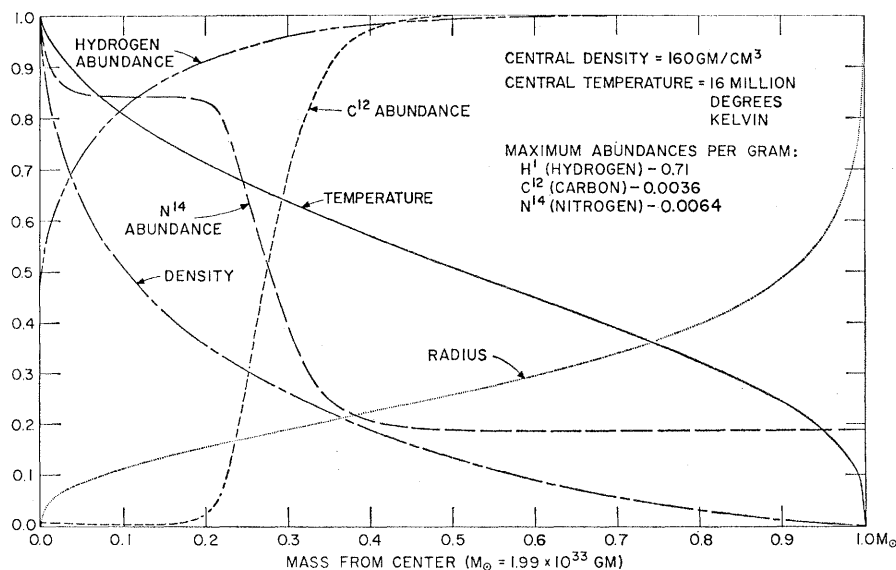


Fig. 3. The approximate distribution of several state and composition variables within the present sun.

larger region, the surface-lithium abundance begins to decrease. Calculations show that, after the star reaches the tip of the red-giant branch, the surface-lithium abundance will be reduced by a factor of at least 60 from the surface-lithium abundance characterizing the star when it leaves the main sequence. From the positions of Capella A and B relative to the  $3-M_{\odot}$  model track in Fig. 2, we may conclude that the lithium abundance at the surface of Capella B should be at least 60 times less than that at the surface of Capella A. This is exactly what is observed (9). Theory also suggests that the surface ratio of  $N^{14}$  to  $C^{12}$  should be about three times larger in Capella B than in Capella A. This prediction has not yet been verified.

For the purpose of testing the overall validity of the theory of stellar structure and evolution, a fruitful approach is to examine, simultaneously, large numbers of stars with a variety of masses and possibly also of different ages. One attempts to discover trends among the observable properties of such stars which are related to mass-dependent or age-dependent characteristics (or both) of a large group of theoretical models of various masses and ages.

The key to the comparison lies in the recognition that, the more rapidly stars pass through a given region of the Hertzsprung-Russell diagram, the lower, in all probability, is the population of stars in this region of the diagram. For example, the number of stars of a given mass in regions of the Hertzsprung-Russell diagram where helium burning in the core occurs should be about four or five times smaller than the number of stars of this same mass near the main sequence in the phase of core hydrogen burning.

Since all stages of nuclear burning subsequent to the phase of helium burning are expected to be of much shorter duration than all prior phases, the only other region of the Hertzsprung-Russell diagram which should be heavily populated is the region occupied by stars in their final stages, after nuclear fuels are exhausted.

In Fig. 4 the shading indicates regions where one expects to find large numbers of stars. The general features of the expected distribution are roughly consistent with the observations.

The overwhelming majority of nearby metal-rich stars lie along the main-

sequence band. Masses for approximately 100 main-sequence stars are known with sufficient accuracy to establish an empirical relationship between mass and luminosity along this band. This relationship is in fair agreement with that predicted theoretically. More careful comparison shows that some of the spread in the observed main sequence is due to differences in initial composition, although most of the spread is due to evolution.

The number of stars along the main sequence is known to be a rapidly decreasing function of increasing luminosity and hence of mass. This is what one expects theoretically from the fact

that the main-sequence lifetime decreases rapidly with increasing mass. For example, the lifetime of a  $1.5-M_{\odot}$  star on the main sequence is approximately 25 times larger than that of a  $5.0-M_{\odot}$  star. If the rate at which  $5-M_{\odot}$  stars are born were equal to the rate at which  $1.5-M_{\odot}$  stars are born, there should be roughly 25  $1.5-M_{\odot}$  stars on the main sequence for every  $5-M_{\odot}$  star.

Along the low-temperature edge of the main sequence is found a class of stars which appear to be emitting matter at a modest rate. Luminous members of this class are called "BE" or "blue, emission" stars. A rational

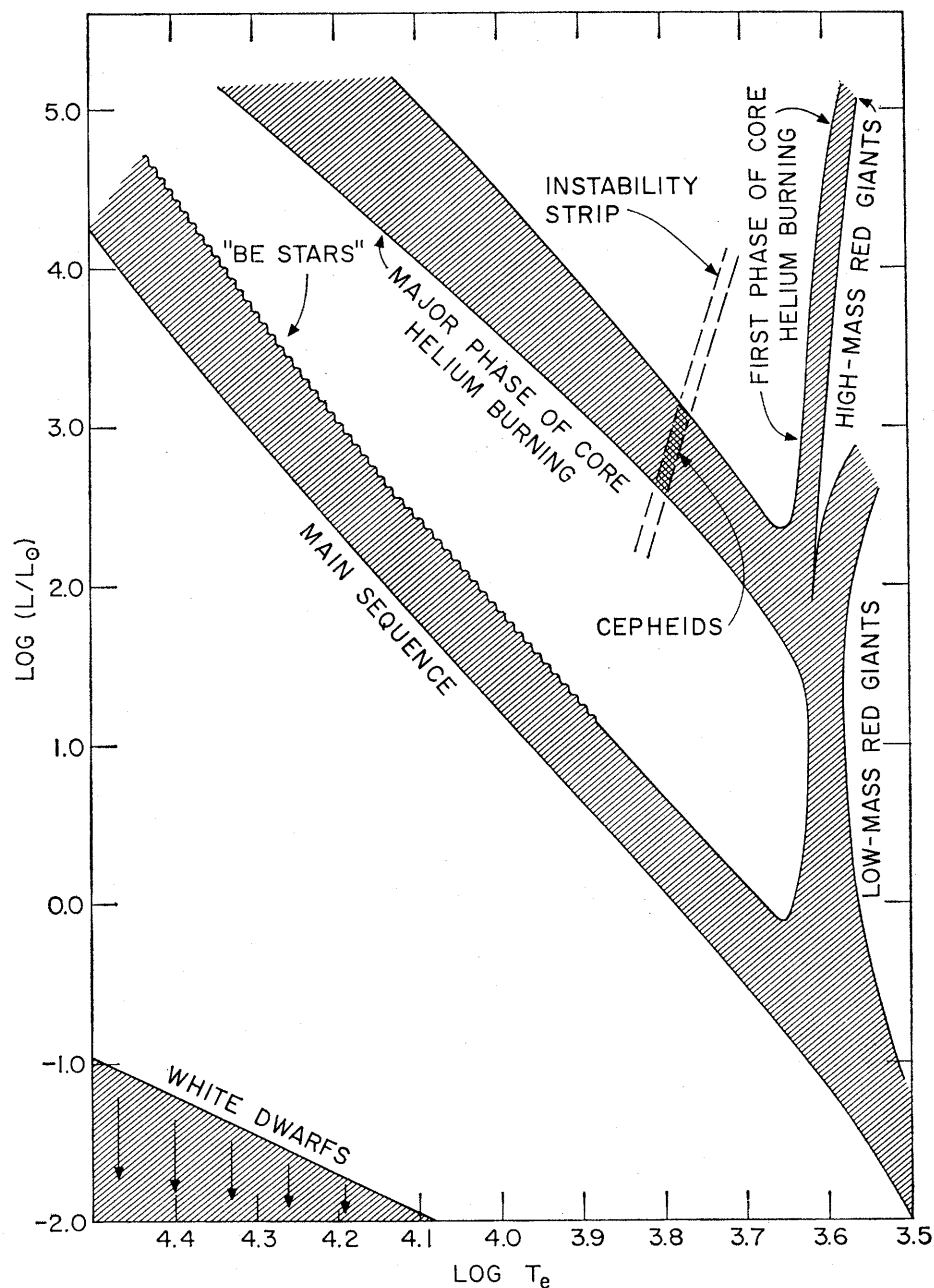


Fig. 4. The distribution of metal-rich stars in the Hertzsprung-Russell diagram expected on the basis of model calculations.  $L$  and  $T_e$  as in Fig. 1.

explanation of the BE stars rests on the observation that luminous, main-sequence stars are in relatively rapid rotation (10). Toward the end of the phase of overall contraction and during the phase of shell development which occurs near the low-temperature edge of the main-sequence band, the core of the star contracts rather suddenly. In order to conserve angular momentum, the star must rotate more rapidly. Beyond a critical rotation frequency the matter near the equatorial regions of the star can no longer be kept in contact with the rest of the star by gravitational forces. Matter is then emitted along the star's equator. The analogy with a child holding on to a more and more rapidly rotating merry-go-round is obvious. Following the shell-development stage, the star alters its structure in such a way that the rotation rate decreases and the process of rapid ejection ceases. Hence one expects to find the BE stars confined to a very narrow region in the Hertzsprung-Russell diagram, as they are observed to be.

Next to main-sequence stars in number are the white dwarfs, a category which embraces a much larger region than is shown in Fig. 4. A quite satisfactory theoretical description of these stars has been available for many years (11). White dwarfs are, as the name implies, highly condensed stars with radii in many cases no larger than the radius of the earth. The condensation is so extreme that, over most of the star's interior, electrons are degenerate and provide most of the supporting interior pressure. Therefore, as the white dwarf evolves, its radius remains essentially constant and independent of the interior temperature distribution. The primary source of escaping energy is the thermal energy of nondegenerate heavy nuclei. As time passes, the white dwarf becomes cooler and luminosity decreases.

The high frequency of white dwarfs in the Galaxy suggests that a large fraction of stars of all masses pass through the white-dwarf phase before becoming completely inactive. The fact that most white dwarfs are characterized by masses of less than  $1 M_{\odot}$  suggests, then, that many stars lose mass prior to becoming white dwarfs. The mechanism of ejection is not known.

Third in frequency of occurrence are the red giants, which have evolved from main-sequence progenitors of

mass less than about  $2.25 M_{\odot}$ . This is what one would expect from the theory, which suggests that metal-rich stars of  $2.25 M_{\odot}$  or less will evolve up the giant branch prior to helium burning in the core and will evolve both down and up the giant branch during the phase of core helium burning.

Another easily understood feature in the distribution of metal-rich stars is the fact that Cepheid variables (luminous stars pulsating with periods between 2 and 50 days) seem to be concentrated at luminosities on the order of 1000 times the sun's luminosity. Calculations show (12) that, at any given luminosity, a stellar envelope may pulsate with large amplitude only if surface temperature lies within a very narrow range. The region within which large-amplitude pulsations may occur is defined in Fig. 4 by dashed lines and is designated "instability strip." Outside of this strip, any artificially induced or remnant pulsation will die away rapidly. The shaded region labeled "major phase of core helium burning" indicates where high-mass stars spend the major fraction of their lives following the main-sequence phase. The intersection of these two strips represents the region where one should *and does* find the bulk of the Cepheids. Through comparison with the evolutionary tracks in Fig. 2, one concludes that most Cepheids have a mass of about 4 to  $5 M_{\odot}$  and are in the phase of core helium burning.

### Comparison with Cluster Stars

One of the most elegant comparisons with the observations that one can attempt involves groups of stars in clusters. The major advantage in dealing with clusters is that all component stars may, to a first approximation, be assumed to be of the same age and initial composition.

The comparison requires the availability of evolutionary tracks for models of different mass but of the same initial composition. These tracks should be viewed in the following fashion. Suppose that, at time zero, all models are on the main sequence. At any given later time,  $t$ , each model will have reached a specific point on its evolutionary track. For every preassigned time  $t$ , these specific points may be joined to form a smooth curve, which may be called the time-constant locus appropriate to time  $t$ .

For example, if  $t$  is chosen to be equal to the main-sequence lifetime of a  $5 M_{\odot}$  star, then that portion of the time-constant locus which is derived by joining points along evolutionary tracks for stars less massive than  $5 M_{\odot}$  will lie within the main-sequence band. That portion derived from tracks of stars slightly more massive than  $5 M_{\odot}$  will lie between the main sequence and the region of red giants. The "turn-off" from the main sequence occurs at that luminosity and surface temperature characterizing the  $5 M_{\odot}$  track as it leaves the main sequence.

For every star in a given cluster, a corresponding position may be assigned in the Hertzsprung-Russell diagram. By drawing a smooth line through the distribution of points in the Hertzsprung-Russell diagram, one obtains an idealized "cluster locus" which may be thought of as an empirical time-constant locus. In principle, by thumbing through a prepared catalog of theoretical time-constant loci, one should come across one which best represents the empirical time-constant locus. The age of the cluster may then be equated with that time  $t$  characterizing the appropriate theoretical locus. To the extent that characteristic features of several cluster loci correspond to characteristic features of the most appropriate theoretical loci, one may have confidence in the completeness of the theory.

Idealized cluster loci describing the distribution of stars in the clusters M67 and NGC188 are shown in Fig. 5 (13). Several features distinguish the M67 locus from the NGC188 locus. In the region between the main-sequence band and the location of red giants (points *D* to *E* and *F* to *G*), stars in M67 are more luminous than stars in NGC188. This means that the stars in M67 which have left the main sequence are more massive than the stars in NGC188 which have left the main sequence. The cluster M67 is therefore younger than NGC188.

Along the M67 locus, the density of stars between points *B* and *C* is considerably less than the density of stars along either the preceding portion, *A-B*, or the following portion, *C-D*. Coupling this knowledge with the fact that theoretical time-constant loci must be continuous, one infers that stars near point *C* are only very slightly more massive than stars near point *B*, and that the rate of evolution between points *B* and *C* is quite large compared with the rate at which

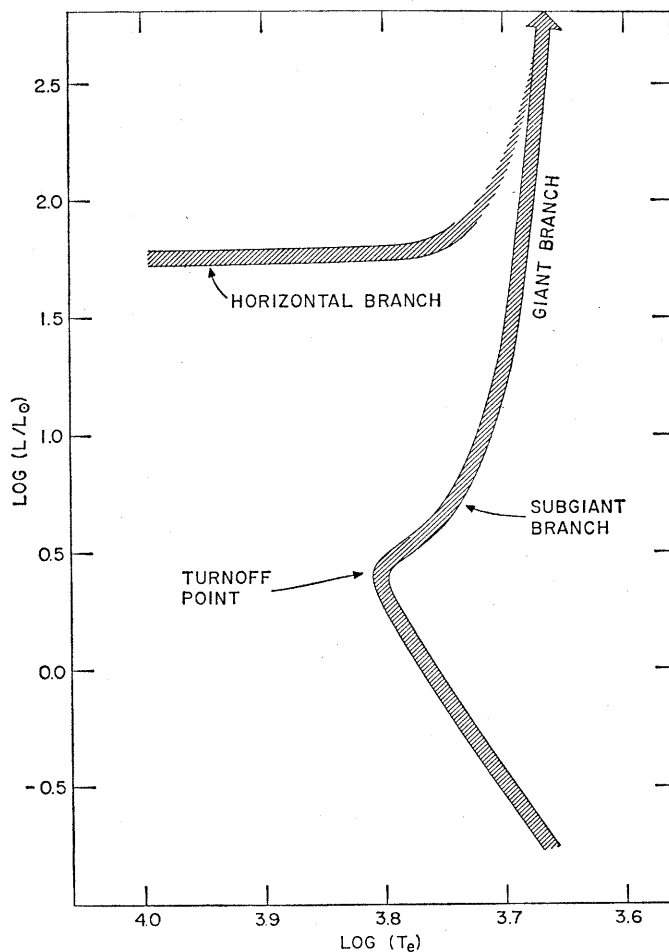
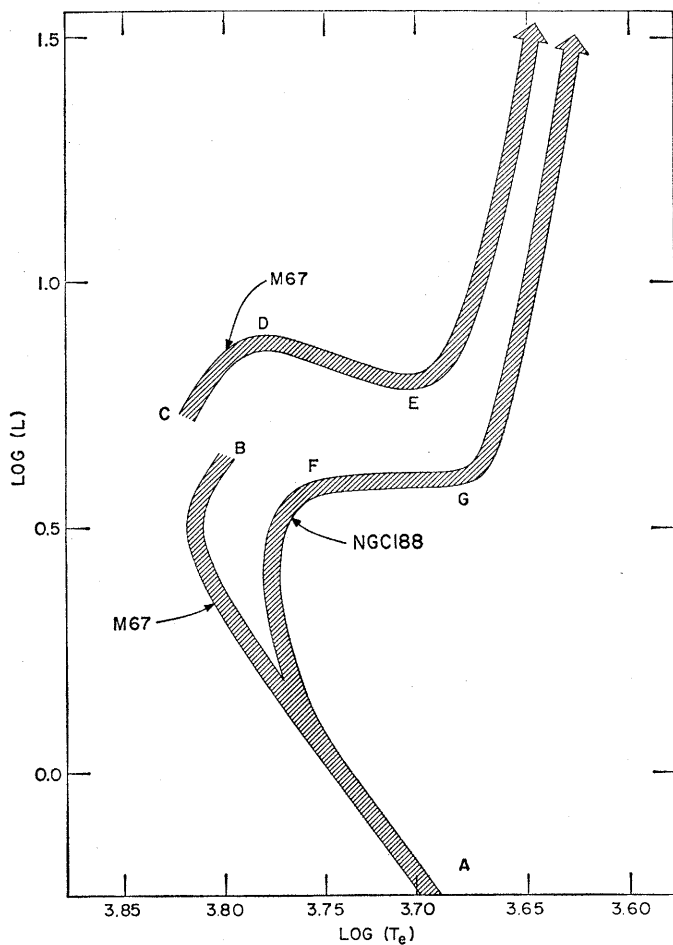


Fig. 5 (left). Schematic cluster loci for stars in the clusters M67 and NGC188.  $L$  and  $T_e$  as in Fig. 1. Fig. 6 (right). Schematic cluster locus for stars in the globular cluster M92.  $L$  and  $T_e$  as in Fig. 1.

stars of this mass either evolve toward point  $B$  or leave point  $C$ . According to the model evolution described in preceding sections, we can identify stars near point  $B$  as ones which are just beginning the phase of overall contraction immediately preceding the complete exhaustion of hydrogen in a convective core. Stars near point  $C$  have just completed this phase and are embarking upon the relatively long phase of hydrogen burning in a thick shell. Stars along the M67 locus between points  $C$  and  $D$  are all burning hydrogen in a thick shell. The absence of a gap in the star density along the NGC188 locus implies that all stars in NGC188 are too light to possess convective cores during the main-sequence phase. We conclude again that M67 contains more massive stars than NGC188 and that therefore NGC188 is older than M67.

By arguments similar to those used above, we identify stars along the loci between points  $D$  and  $E$  and between  $F$  and  $G$  as stars experiencing a rapid reduction in the thickness of the

hydrogen burning shell. We have already seen that the drop in luminosity during the shell-narrowing phase (points 4 to 5 in Fig. 2) decreases as stellar mass is decreased. We infer once more that M67 contains more massive stars and is younger than NGC188.

Ideally, I should prepare theoretical time-constant loci for quantitative comparison with the cluster loci. Unfortunately, this would require the construction of many more evolutionary tracks than are shown in Fig. 2. In lieu of doing this, I have elsewhere (14) compared cluster loci and the evolutionary tracks for those two available model stars whose masses ( $1.25 M_{\odot}$  and  $1 M_{\odot}$ ) correspond most closely to the most massive stars in M67 and in NGC188, respectively. By interpolating between the characteristics of the  $1-M_{\odot}$  and  $1.25-M_{\odot}$  tracks, I find that the age of M67 is roughly  $(5.5 \pm 1) \times 10^9$  years, whereas the age of NGC188 is roughly  $(11 \pm 2) \times 10^9$  years.

The age of  $11 \times 10^9$  years estimated for NGC188 is close to the age of

the universe as deduced from the red shift experienced by light from distant galaxies. Depending upon the particular cosmological arguments used, the so-called Hubble time implies an age for the universe somewhere in the range  $(8-13) \times 10^9$  years. The stars in NGC188 were therefore formed only a few billion years after the universe began to expand.

It is encouraging that the details of cluster loci and many regularities in the distribution of nearby metal-rich stars can be accounted for in terms of the properties of calculated stellar models. The basic physics involved in the construction of these models must therefore be reasonably complete.

#### Conundrums Posed by Metal-Poor Stars

As I have pointed out, most of the stars in our galaxy are characterized by surface abundances of heavy elements that are many times smaller than abundances of these elements at the

surface of the sun. It is astonishing that, until quite recently, it has not been possible to make any comparably definite statements concerning the relative abundance of helium in these stars. The reason for this is that the great majority of metal-poor stars possess a surface temperature which is too low to permit a meaningful spectroscopic determination of the surface abundance of helium. In addition, there are no binary systems of metal-poor stars close enough to the sun to permit a *direct* determination of stellar mass. It is therefore impossible to make an unambiguous estimate of initial helium content by fitting to models of fixed mass but of variable initial helium content.

In a recent effort to dispel the uncertainty concerning initial helium

abundance, John Faulkner of the California Institute of Technology and I have compared evolutionary tracks of evolving metal-poor model stars with the distribution of groups of metal-poor stars in the Hertzsprung-Russell diagram (14). By altering the initial helium and hydrogen abundances in the models, distinct variations are produced in the evolutionary tracks and in the rate of travel along these tracks. By making comparisons with the distribution (in the Hertzsprung-Russell diagram) of metal-poor stars found in clusters, we are then able to make statements concerning the relative merits of a particular choice of initial helium abundance.

In Fig. 6, a schematic locus for the typical metal-poor cluster M92 is shown (15). The most distinctive fea-

ture of this locus is the strongly populated region designated "horizontal branch," a feature which is definitely not apparent in loci for clusters composed of metal-rich stars.

In Figs. 7 and 8, evolutionary tracks for a selection of metal-poor models are depicted. The solid lines represent tracks for stars evolving off the appropriate metal-poor main sequence during stages of pure hydrogen-burning. For the initial main-sequence models described in Fig. 7, helium comprises 35 percent of the star's mass and hydrogen comprises 65 percent. For the corresponding models in Fig. 8, helium and hydrogen comprise, respectively, 10 and 90 percent of the star's mass. In both cases the heavy-element abundance has been chosen to be exactly 100 times smaller than that

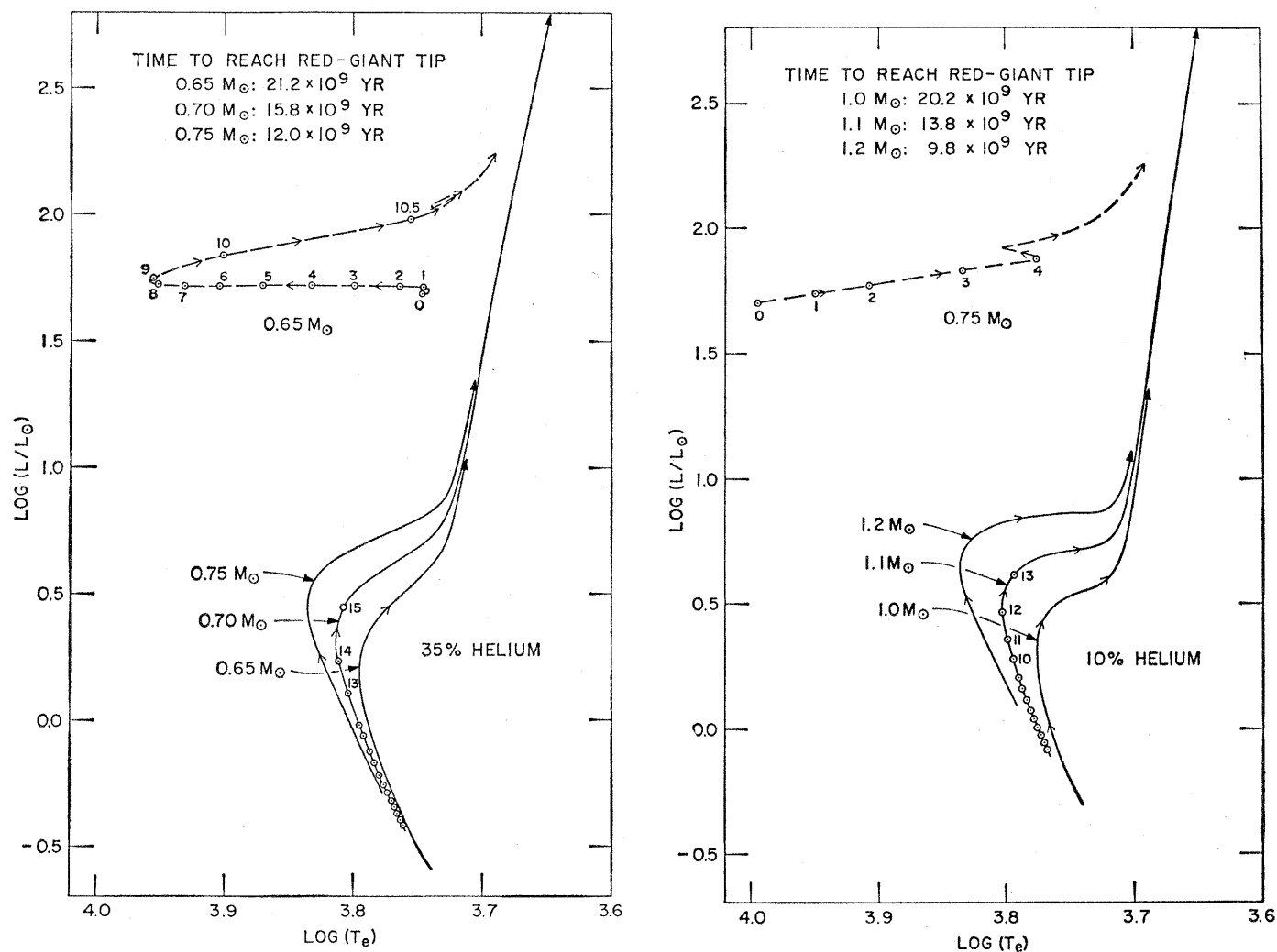


Fig. 7 (left). Evolutionary paths for metal-poor stars with a high initial abundance of helium. Helium is assumed to comprise, initially, 35 percent of each star's mass when it first reaches the main sequence. Intervals between consecutive circles along the track for the 0.7- $M_{\odot}$  model correspond to evolutionary times of  $10^9$  years. Intervals between circles along the dashed track for the 0.65- $M_{\odot}$  model correspond to  $10^7$  years.  $L$  and  $T_e$  as in Fig. 1. Fig. 8 (right). Evolutionary paths for metal-poor stars with a low initial abundance of helium. Helium comprises, initially, 10 percent of each star's mass. Intervals between consecutive circles along the track for the 1.1- $M_{\odot}$  model correspond to evolutionary times of  $10^9$  years. Intervals between circles along the dashed track for the 0.75- $M_{\odot}$  model correspond to  $10^7$  years.  $L$  and  $T_e$  as in Fig. 1.

chosen for the metal-rich stars already discussed.

In each case, model masses have been chosen in such a way as to achieve "best" fits with the cluster locus in the neighborhood of the "turnoff" point and the "subgiant" branch.

If the higher of the two choices for initial helium is correct, the most massive stars in the cluster M92 are in the mass range ( $0.65 \rightarrow 0.75$ )  $M_{\odot}$ . If one assumes the smaller of the two choices, the most massive stars in M92 are in the range ( $1.0 \rightarrow 1.2$ )  $M_{\odot}$ .

A more satisfactory comparison of the models with the cluster locus involves the construction of theoretical time-constant loci. Such a comparison has been made (16), with the result that, for both choices of initial helium content, the derived age for M92 is in the neighborhood of  $15 \times 10^9$  years, the exact figure depending on the assumed initial helium abundance. However, a better fit with the *shape* of the M92 locus is achieved with the higher initial helium abundance. That a better fit may be achieved with the higher-helium models is evident also from the shape of individual tracks in Figs. 7 and 8.

An age of 15 billion years is uncomfortably large when it is compared with the age of the universe suggested by current estimates of the Hubble time. This may mean that there exists an error (i) in the chain of observational and theoretical arguments which give the Hubble time, (ii) in the current cosmological interpretation of this time, (iii) in the evolutionary models, or (iv) in the manner in which observations are compared with the stellar models. In any case, metal-poor stars are certainly among the oldest objects in our galaxy, and a statement concerning the initial helium abundance in these stars is simultaneously a statement about the abundance of helium in our galaxy when stars first began to form.

For both choices of initial helium content, evolution continues along the giant branch until helium is ignited explosively in the electron-degenerate core. Immediately after the helium flash, the mass contained in the hydrogen-exhausted core depends primarily on the ratio of helium to hydrogen in the region outside of the hydrogen-burning shell and is relatively independent of total stellar mass. When 35 percent of the matter outside of the

hydrogen-exhausted core is helium, the mass of the helium core is roughly  $0.4 M_{\odot}$  at the end of the flash phase. When the stellar envelope is 10 percent helium, the corresponding core mass is roughly  $0.6 M_{\odot}$ .

The dashed line in Fig. 7 represents the evolutionary track of a metal-poor star of mass  $0.65 M_{\odot}$  during the phase of core helium burning, after core degeneracy has been "lifted." In the initial model the mass of the hydrogen-exhausted core is  $0.4 M_{\odot}$  and helium comprises 35 percent of the mass of the region between the hydrogen-burning shell and the surface. During the major portion of the evolution shown, the rate at which energy is generated by the conversion of hydrogen into helium in the shell is higher than the rate of energy generation by helium burning in the core, and the model star evolves to higher surface temperatures. When the rate of energy generation in the core begins to exceed that of energy generation in the shell, the star begins to evolve more rapidly back to lower surface temperatures. Note that the mass of the star which evolves in the neighborhood of the cluster horizontal branch is roughly the same as the mass of the stars along the cluster giant branch, as deduced from a comparison with models evolving during stages of pure hydrogen-burning.

Choosing an envelope-helium abundance of 10 percent by mass, one finds that, following the helium flash, models of total mass greater than  $0.6 M_{\odot}$  evolve toward lower surface temperatures during the major portion of the phase of core helium burning. In these models the hydrogen-burning shell is essentially inactive and the luminosity of the model is supplied solely by the conversion of helium into carbon and oxygen near the stellar center.

We have seen that, on the basis of fits with models evolving off the main sequence during hydrogen-burning phases, stars beyond the turnoff point in M92 may be assigned masses in the range 1 to  $1.2 M_{\odot}$ , for the lower of the two choices of initial helium. Surprisingly, models of this mass evolve nowhere near the horizontal branch during the phase of core helium burning. *Only by choosing model mass considerably lower than  $1 M_{\odot}$*  can an approximate fit with the horizontal branch be achieved. An approximate fit is illustrated by the dashed

line in Fig. 8, which represents the track of an  $0.75 M_{\odot}$  model during the phase of core helium burning.

If, then, one adopts the lower of the two choices of initial helium content, it is necessary to assume that 30 to 40 percent of a star's mass is lost between the main-sequence phase and the onset of the horizontal-branch phase. There are two likely mechanisms for this mass loss: (i) a quiet "stellar-wind" expulsion of mass, which is expected to become increasingly more important at lower surface temperatures and hence to be most effective along the giant branch; (ii) an expulsion of mass via shock waves generated in the stellar core as a result of the helium flash. Unfortunately, no quantitative understanding of either of these mechanisms exists, and it is impossible to predict either rates of quiet mass loss or the quantity of matter ejected as a result of shocks. Furthermore, observational estimates of mass loss are extremely difficult to make, and results are inconclusive. The choice of a low initial abundance of helium thus forces us to invoke a substantial mass loss which we are not capable of calculating or observing directly.

From the fact that horizontal-branch models with low envelope helium (Fig. 8) and high envelope helium (Fig. 7) evolve in almost exactly opposite directions, it is clear that, for intermediate choices of envelope helium content, models would evolve in intermediate directions, and that, for an envelope helium abundance of approximately 20 percent by mass, models would evolve vertically at nearly constant surface temperature during the phase of core helium burning. It is further clear that a choice of envelope helium content closer to 0 percent would lead to an even more horizontal track during helium burning than is given by a choice of 10 percent. Thus, one firm conclusion is that the initial abundance of helium must be in one of two ranges: ( $35 \pm 5$ ) percent by mass or ( $5 \pm 5$ ) percent by mass.

On the basis of an argument which involves a comparison between model lifetimes and the density of stars in various portions of diagrams of metal-poor clusters, Dr. Faulkner and I concluded approximately a year ago that the weight of evidence favored the choice of the higher initial abundance of helium.

During the past year, several spec-

troscopists (17) have investigated a number of nearby field stars of low metal content which appear to possess luminosities and surface temperatures comparable to those at the high-temperature end of the horizontal branch in metal-poor clusters. Preliminary results suggest that the helium abundance at the surfaces of these stars is less than 1 or 2 percent by mass. If this conclusion is borne out by further observation and analysis, then astrophysicists may be faced with the major tasks of (i) elaborating a quantitative theory of mass loss either by solar-wind mechanisms or by shocks originating in the helium flash (or both), and (ii) refining the theory of energy flow (including mass loss) so as to remove the discrepancy between theoretical time-constant loci, as derived from low-helium models, and loci for metal-poor clusters.

On the other hand, it has recently been argued (18) that the apparent low abundance of helium relative to hydrogen at the surfaces of stars near the blue end of the horizontal branch may be due to the fact that, under the influence of gravity, the heavier atoms of helium diffuse inward from the surface and are thus lost from view. In most other stars, the tendency for heavier elements to sink inward from the surface is counterbalanced either by convective mixing (when the star possesses a convective envelope) or by a rotationally induced circulation of matter in envelope regions (all

real stars rotate to some extent). Stars at the blue end of the horizontal branch do not rotate very rapidly and do not possess convective envelopes, so that diffusion may well deplete the surface abundance of helium and thereby invalidate any attempt to gauge directly the abundance of helium below the surface. Hence it would seem that nature is conspiring to prevent the astronomer from knowing too easily the answer to that most important question: What was the initial helium abundance in our galaxy when the oldest, metal-poor stars were formed?

#### References and Notes

1. A much more detailed account of the evolution of a  $5-M_{\odot}$  star may be found in I. Iben, Jr., *Astrophys. J.* **143**, 483 (1966).
2. The most recent summary of the reactions involved in the  $p-p$  processes is P. D. Parker, J. N. Bahcall, W. A. Fowler, *Astrophys. J.* **139**, 602 (1964). Descriptions of the CN-cycle reactions are given by E. M. Burbidge, G. R. Burbidge, W. A. Fowler, and F. Hoyle, *Rev. Mod. Phys.* **29**, 547 (1957), and by H. Reeves, in *Stellar Structure*, L. H. Aller and D. B. McLaughlin, Eds. (Univ. of Chicago Press, Chicago, 1965).
3. The surface temperature, radius  $R$ , and luminosity of a star are related by the equation  $\sigma T_e^4 = L/4\pi R^2$ , where  $\sigma$  is the Stefan-Boltzmann constant.
4. The triple-alpha process is described in E. M. Burbidge *et al.*, *Rev. Mod. Phys.* **29**, 547 (1957) and in H. Reeves, in *Stellar Structure*, L. H. Aller and D. B. McLaughlin, Eds. (Univ. of Chicago Press, Chicago, 1965).
5. Calculations have been carried further by a group in Germany consisting of E. Hofmeister, R. Kippenhahn, H. C. Thomas, and A. Weigert. See, for example, *Z. Astrophys.* **60**, 57 (1964); *ibid.* **61**, 241 (1965).
6. I. Iben, Jr., *Astrophys. J.* **140**, 1631 (1964); *ibid.* **141**, 993 (1965); *ibid.* **142**, 1447 (1965); *ibid.* **143**, 483 (1966); *ibid.*, p. 505; *ibid.*, p. 516; *ibid.*, in press.
7. Over most of the stellar interior, electrons behave like classical particles and matter obeys

Boyle's law. The pressure due to electrons is directly proportional to both temperature and density. At very high densities, however, electrons begin to exhibit quantum characteristics, one of which is that no two electrons may be found in the same energy state. The pressure due to electrons becomes proportional to the five-thirds power of the density and nearly independent of the temperature. The electrons are said to be degenerate.

8. R. L. Sears, *Astrophys. J.* **140**, 477 (1964).
9. G. Wallerstein, *Nature* **204**, 367 (1964); *Astrophys. J.* **143**, 823 (1966).
10. The argument presented here is that of Theodore Schmidt-Kaler and also of J. Crampin and F. Hoyle, *Monthly Notices Roy. Astron. Soc.* **120**, 33 (1960).
11. See, for example, S. Chandrasekhar, *An Introduction to Stellar Structure* (Univ. of Chicago Press, Chicago, 1939).
12. N. Baker, in *Star Evolution*, L. Gratton, Ed. (Academic Press, New York, 1963), p. 369.
13. Surface temperature and luminosity are not determined directly from observations. The cluster loci in Fig. 5 are estimates, obtained after theoretical transformations have been performed on observational data. Observational data for M67 are given by H. L. Johnson and A. Sandage, *Astrophys. J.* **121**, 616 (1955); those for NGC188 are given by A. Sandage, *ibid.* **135**, 333 (1962).
14. J. Faulkner and I. Iben, Jr., *ibid.* **144**, 995 (1966).
15. Although relative surface temperatures and luminosities along the locus in Fig. 6 may be approximately correct inferences from the observations, the absolute value of the surface temperature (in addition to the luminosity) for any star may be considerably in error. Observational data from A. Sandage and M. F. Walker, *Astrophys. J.* **143**, 313 (1966) and from A. Sandage and L. L. Smith, *ibid.* **144**, 886 (1966), have been used.
16. I. Iben, Jr., and J. Faulkner, in preparation.
17. L. Searle and A. W. Rodgers, *Astrophys. J.* **143**, 809 (1966); J. L. Greenstein, *ibid.* **144**, 496 (1966); W. L. W. Sargent and L. Searle, *ibid.* **145**, 652 (1966).
18. G. S. Greenstein, J. W. Truran, A. G. W. Cameron, private communication.
19. The work described in this article has been supported in part by the National Aeronautics and Space Administration (NSG-496) and in part by the National Science Foundation (GP-6387). The discussion presented here is a summary of lectures given by the author for the Summer Faculty Program in Space Physics, held under the auspices of Columbia University at the NASA Institute for Space Studies, New York, 7-13 July 1966.

## Coordinated Planning for Science in Communist Europe

Council for Economic Mutual Assistance coordinates national policies and plans in science and technology.

Lloyd F. Jordan

The role of the Council for Economic Mutual Assistance (CEMA) in coordinating policy and planning in support of scientific and technical collaboration of its members has grown

steadily since 1956. The Council has made considerable headway, especially since 1962, yet several problems continue to impede its efforts in this sphere. Both the progress achieved by

and the problems confronting CEMA in such coordination are important developments that merit consideration by those concerned with integration in Eastern Europe and with international scientific and technical collaboration in general.

In January 1949 the U.S.S.R. and its satellites met in Moscow and organized CEMA (1); other charter members were Bulgaria, Czechoslovakia, Hungary, Poland, and Rumania, while Albania joined almost immediately and East Germany joined in the autumn of 1950 (2). Since December 1961 Albania has not actively participated because of its strained relations with the U.S.S.R. (3). In 1962 Mongolia changed in status from observer to full member. Communist China, North

The author, a former federal executive fellow, is a political scientist and specialist on East European affairs with the U.S. Central Intelligence Agency.